C. R. Mecanique 342 (2014) 382–388

Contents lists available at ScienceDirect

Comptes Rendus Mecanique

www.sciencedirect.com

Separation flow control

Upstream open loop control of the recirculation area downstream of a backward-facing step

Nicolas Gautier, Jean-Luc Aider *

Laboratoire de physique et mécanique des milieux hétérogènes (PMMH), UMR7636 CNRS, École supérieure de physique et chimie industrielles de la Ville de Paris, 10, rue Vauquelin, 75005 Paris, France

ARTICLE INFO

Article history:
Received 30 August 2013
Accepted 29 November 2013
Available online 10 June 2014

Keywords:
Flow control
Open loop control
Pulsed jets
Upstream actuation
Backward-facing step
Duty-cycle

ABSTRACT

The flow downstream a backward-facing step is controlled using a pulsed jet placed upstream of the step edge. Experimental velocity fields are computed and used to quantify the recirculation area. The effects of jet amplitude, frequency and duty cycle on this recirculation area are investigated for two Reynolds numbers ($Re_h = 2070$ and $Re_h = 2900$). The results of this experimental study demonstrate that upstream actuation can be as efficient as actuation at the step edge when exciting the shear layer at its natural frequency. Moreover, it is shown that it is possible to minimize both jet amplitude and duty cycle and still achieve optimal efficiency. With minimal amplitude and a duty-cycle as low as 10%, the recirculation area is nearly canceled.

1. Introduction

Separated flows are ubiquitous in nature and industrial processes. They occur in many devices such as combustion chambers, air conditioning plants, moving ground and air vehicles (see [1–3]). The main feature of separated flows is the recirculation bubble, i.e. the region where the direction of the flow is reversed [4]. In most industrial applications, it is important to reduce recirculation in order to improve drag, increase lift, suppress vibrations, or lower aeroacoustic noise. Sometimes, an increase in recirculation is welcome, for instance to increase mixing in a combustion chamber.

The Backward-Facing Step (BFS) flow is a benchmark problem, and is commonly used to study massively separated flows both numerically and experimentally (see [4–7]). The main features of the BFS flow are the creation of a recirculation downstream of the step together with a strong shear layer in which Kelvin–Helmholtz instability can trigger the creation of spanwise vortices (Fig. 1a). Because separation of the boundary layer is imposed by the step edge, flow control strategies are also limited: it is not possible to delay or trigger the flow separation, but only to force the shear layer in a different state to modify the overall recirculation and location of the reattachment point [8].

There are many ways of controlling separated flows, as detailed by Fiedler and Fernholz [9]. Both passive and active actuation methods have been the subject of much research [10,11]. Active actuations using either pulsed or synthetic jets are always located at the step edge in order to ensure maximum effect on the shear layer. Furthermore, this is only possible for geometries where the separation line is well-defined, which is not the case for rounded walls or ramps. While this is effective, it does burden any setup with additional engineering constraints. For academic purposes, this is of lesser concern, while for industrial purposes the cost of spatially imposed actuation can be prohibitive. Furthermore, it has been shown

* Corresponding author.
E-mail address: aider@pmmh.espci.fr (J.-L. Aider).

http://dx.doi.org/10.1016/j.crme.2014.05.004
1631-0721/

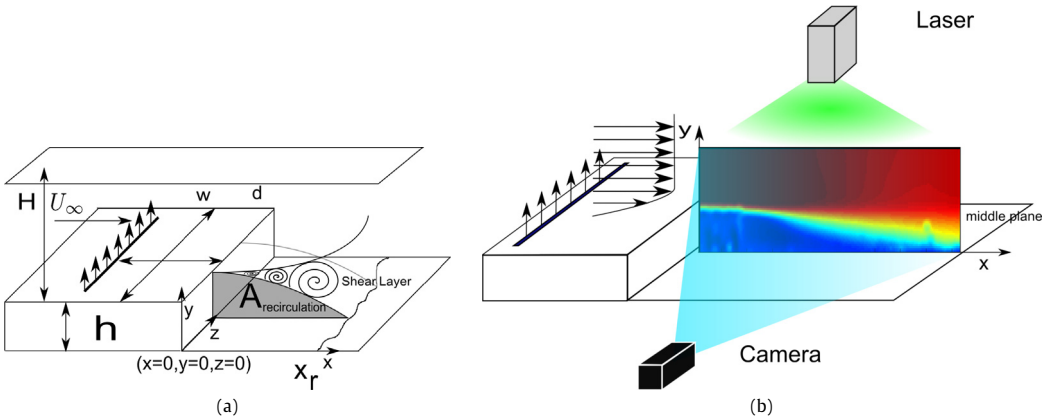

Fig. 1. (Color online) (a) Sketch of the BFS geometry and definition of the main parameters. (b) Sketch of the acquisition apparatus.

that for geometries where the separation point can move because of a change in external conditions, the effectiveness of flow control can be lowered because actuation is no longer where the flow is most receptive [12]. Therefore, knowing where actuation can be placed upstream while retaining effectiveness is of particular interest. Because of its ability to excite instabilities in the shear layer, pulsed actuation is most efficient when controlling separated flows, as has been shown in [10,13,14] and used in [15,16,10]. Pulsed jets actuations are defined by several parameters. However, while the influences of jet amplitude and frequency are always modified, signal shape and duty cycle are seldom investigated.

An important step in most of closed-loop control strategies is choosing one or several control parameters. The parameter should be either directly computable from sensor data, such as local pressure or drag measurement, or obtained by combining sensor data and a model. The model for closed-loop actuation can be simple ([16] recover recirculation length via its correlation to pressure fluctuations) or complicated ([17] recovers an approximation of the flow state through Kalman filtering). In the case of the BFS flow, sensors are most often pressure or skin friction sensors, and the control variable is usually the recirculation length X_r (see Fig. 1a). Wall-based sensors present the advantage of high-frequency acquisition; however, they give a limited view of the flow: many phenomena are difficult to access because they are buried in noise or simply unobservable because vortices in the flow are not visible by wall sensors.

The velocity fields can be analyzed to yield a recirculation *area* instead of a length, as show in [18]. It is a measure of how much recirculation is present in a 2D slice of the flow. While the behavior of the recirculation area is often similar to the recirculation length, it is not always the case. Because more information about the flow is used to compute the recirculation area, it makes sense to use such a variable whenever possible.

In this paper we investigate the effect of an upstream pulsed jet on the recirculation area downstream of a BFS. The flow state is characterized in the middle plane using real-time optical flow measurements. The parametric space formed by jet amplitude, frequency, and duty cycle is explored for two Reynolds numbers.

2. Experimental setup

2.1. Water tunnel

Experiments were carried out in a hydrodynamic channel in which the flow is driven by gravity. The flow is stabilized by divergent and convergent sections separated by honeycombs. The test section is 80 cm long, with a rectangular cross section 15 cm wide and 10 cm high.

The quality of the main stream can be quantified in terms of flow uniformity and turbulence intensity. The standard deviation σ is computed for the highest free stream velocity featured in our experimental setup. We obtain $\sigma = 0.059\ \mathrm{cm\,s^{-1}}$, which corresponds to turbulence levels of $\frac{\sigma}{U_\infty} = 0.0023$.

The mean free stream velocity U_∞ can go up to 22 $\mathrm{cm\,s^{-1}}$. The Reynolds number is based on the step height h, $Re_h = \frac{U_\infty h}{\nu}$, ν being the kinematic viscosity. A specific leading-edge profile is used to smoothly start the boundary layer which then grows downstream along the flat plate, before reaching the edge of the step 33.5 cm downstream. The boundary layer is laminar and follows a Blasius profile. The boundary layer thickness is $\delta = 0.75$ cm for $Re_h = 2070$ and $\delta = 0.89$ cm for $Re_h = 2900$.

2.2. Backward-facing step geometry

The backward-facing step geometry and the main geometric parameters are shown in Fig. 1a. The height of the BFS is $h = 1.5$ cm. The channel height is $H = 7$ cm for a channel width $w = 15$ cm. One can define the vertical expansion ratio $A_y = \frac{H}{h+H} = 0.82$ and the spanwise aspect ratio $A_z = \frac{w}{h+H} = 1.76$.

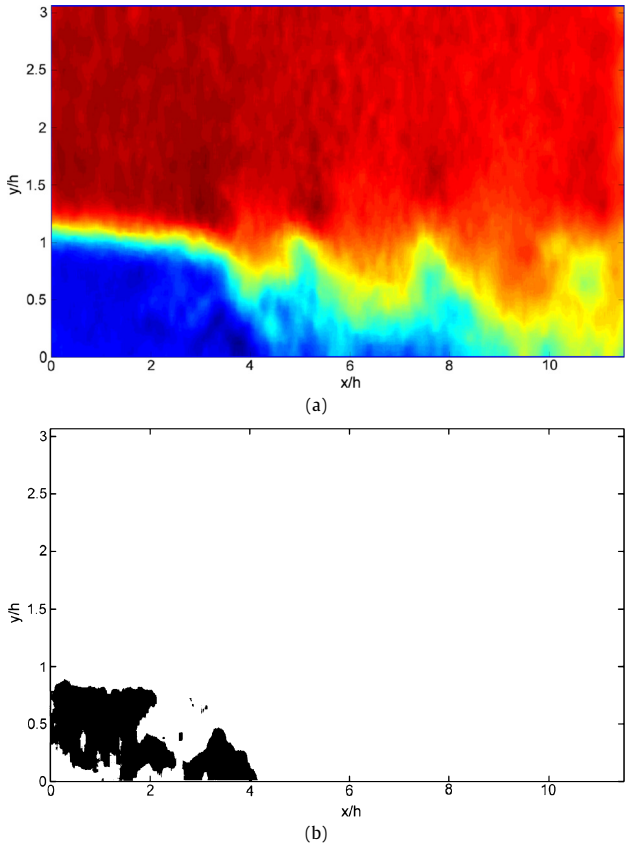

Fig. 2. (Color online) (a) Longitudinal velocity field, $Re_h = 2900$, no actuation. (b) Corresponding instantaneous recirculation area in black using Eq. (1).

2.3. Velocity fields computation

The flow is seeded with 20-μm neutrally buoyant polyamid seeding particles. The vertical symmetry plane of the test section is illuminated by a laser sheet created by a 2 W continuous CW laser beam operating at wavelength $\lambda = 532$ nm passing through a cylindrical lens (Fig. 1b). The pictures of the illuminated particles are recorded using a Basler acA 2000–340 km 8-bit CMOS camera. The camera is controlled by a camera-link NI PCIe 1433 frame grabber. Velocity-field computations are run in real time using the GPU of a Gforce GTX 580 graphics card.

The two components of the planar velocity fields (U, V being respectively the streamwise and vertical components) are computed in real time using an optical flow algorithm [19]. Its offline accuracy has been demonstrated in [20]. Although there are differences with classic PIV algorithms, the output velocity-field resolution is still tied to the size of the interrogation window. However, the output field is dense (one vector per pixel), giving better results in the vicinity of edges and obstacles, which is crucial in BFS flows. Furthermore, this gives exceptionally smooth fields. The algorithm was used by [21,22,18].

2.4. Relationship between recirculation length and area

In the case of separated flows, specifically backward-facing step flows, the recirculation length X_r is commonly used as the input variable [16,10]. There are many ways of computing the recirculation length; however, they all give qualitatively similar results [4]. Because 2D two-component velocity fields are measured, the recirculation area can be characterized by its area instead of its length [18]. Building upon 1D definitions, the recirculation area can be considered to be the area occupied by the region(s) of flow where longitudinal velocity is negative. The instantaneous recirculation area A_{rec} is then defined in Eq. (1):

$$A_{\text{rec}}(t) = \int_A H(-v_x)\,\mathrm{d}a \tag{1}$$

where H is the Heaviside function. Figs. 2a and 2b show an example of an instantaneous recirculation area. In the following, we will consider the mean recirculation area, i.e. A_{rec} is computed for every time step for each instantaneous velocity field before being averaged. It should be noted that it is different from the recirculation area of the mean velocity field.

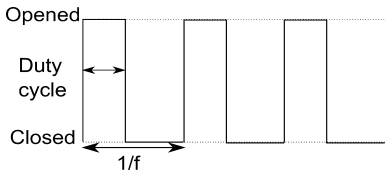

Fig. 3. Square-wave signal and definition of duty-cycle.

Because the recirculation area is computed from 2D data, it has the potential for giving a more accurate measure of recirculation in the flow than the recirculation length.

It has been shown by Gautier and Aider [18] that the recirculation area behaves similarly to the recirculation length for varying Reynolds numbers. Moreover, previous studies [4] have shown that the evolution of the recirculation length as a function of the Reynolds number reaches a maximum between $600 < Re_h < 1000$ before reaching its asymptotic value for $Re_h > 2000$. The Reynolds numbers featured in this study are high enough to ensure that the recirculation area has reached its asymptotic regime where the recirculation length no longer depends on the Reynolds number. For each flow configuration, the recirculation area was computed and recorded over 5 min with a sampling frequency $f_a = 70$ Hz to ensure convergence. The time series is then averaged over time. It should be noted that the recirculation area is computed in real time, concurrently with image acquisition; therefore, only the recirculation area is saved. It avoids saving images and velocity fields, making experimental data very light and greatly hastening data processing and analysis.

2.5. Actuation

Actuation is provided by a flush slot jet, 0.1 cm long and 9 cm wide. Injection is normal to the wall. The slot is located at a distance $d = 3.5$ cm $= 2.11h$ upstream of the step edge (Fig. 1a). Water coming from a pressurized tank enters a plenum and goes through a volume of glass beads designed to homogenize the incoming flow. Jet amplitude is controlled by changing tank pressure. The injection geometry was chosen to keep the perturbation as bi-dimensional as possible.

The flow is modulated by a one-way voltage-driven solenoid valve. It is controlled by a square-wave signal described in Fig. 3, with an actuation frequency f_a. The square-wave signal was chosen for its simplicity, but other signal forms could be considered.

The duty-cycle dc (in %) is the ratio between the time for which the valve is opened over the time of a cycle. Jet amplitude is defined as the ratio between mean jet exit velocity when the jet is active and cross flow velocity $a_0 = \frac{U_{jet}}{U_0}$. The duty cycle therefore has no impact on jet amplitude.

2.6. Natural shedding frequency

Kelvin–Helmholtz instabilities in the shear layer create spanwise vortices that in turn influence the recirculation area. An effective way of detecting such vortices is to compute, on the two-component 2D velocity fields, the swirling strength criterion λ_{Ci} (s^{-1}). It was first introduced by Chong et al. [23], who analyzed the velocity gradient tensor and proposed that the vortex core be defined as a region where $\nabla\mathbf{u}$ has complex conjugate eigenvalues. For 2D data, we have $\lambda_{Ci} = \frac{1}{2}\sqrt{4\det(\nabla\mathbf{u}) - \mathrm{Tr}(\nabla\mathbf{u})^2}$ when such a quantity is real, else $\lambda_{Ci} = 0$. It was later improved and used for the identification of vortices in three-dimensional flows by Zhou et al. [24].

The shedding frequency is obtained by spatially averaging λ_{Ci} in the vertical direction at $x = 3h$, with a sampling frequency $f_s = 40$ Hz. Essentially vortices are counted as they pass through an imaginary line. Fig. 4 shows frequency spectra obtained by Fourier transform for both Reynolds numbers, where $St_h = \frac{fh}{U_0}$ is the Strouhal number based on the step height.

3. Results

3.1. Influence of frequency

Fig. 5 shows the evolution of the recirculation area (non-dimensionalized by the uncontrolled recirculation area A_0) when frequency varies for both Reynolds numbers. Jet amplitude and duty cycle are kept constant. Jet amplitudes were chosen empirically. Previous open-loop control experiments have shown a reduction in the circulation length of up to 40% [10]. Here the recirculation area is decreased by as much as 80%. The reduction is maximum when the pulsing frequency is close to the vortex shedding frequency, $f \simeq f_0$, i.e. $F^+ = \frac{f_a}{f_0} \approx 1$. This result is similar to the effect of flow control at the step edge.

These results show how upstream actuation can effectively control a backward-facing step flow. The influence of the upstream location of the actuator was beyond the scope of the present study.

3.2. Influence of jet exit velocity

Fig. 6 shows the evolution of the recirculation area when jet amplitude varies for both Reynolds numbers. The actuation frequency giving the maximum reduction was chosen for both Reynolds numbers ($F^+ \approx 1$), and the duty cycle was kept constant at $dc = 50\%$. One

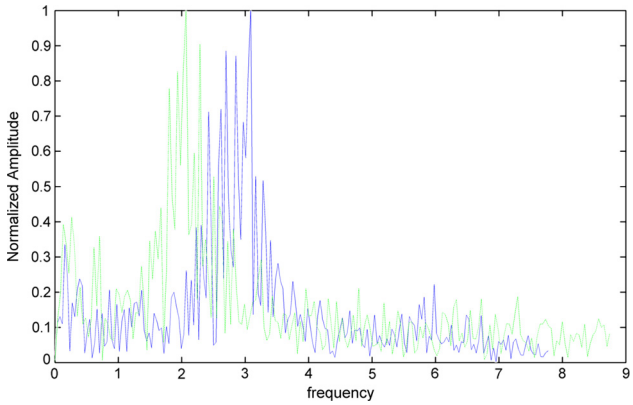

Fig. 4. (Color online) Frequency spectrum for $Re_h = 2070$ (peak at $St_h = 0.258$) in dashed green and for $Re_h = 2900$ (peak at $St_h = 0.272$) in solid blue.

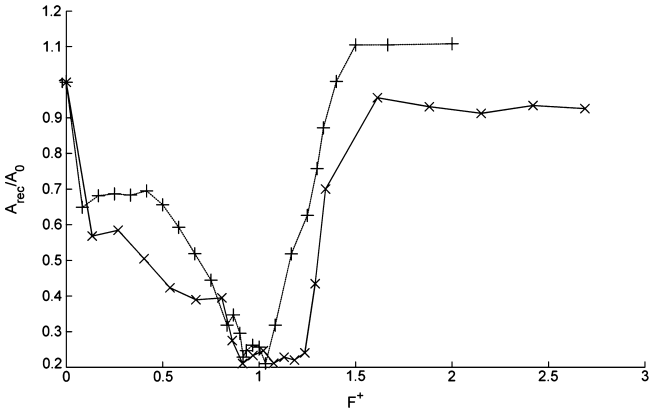

Fig. 5. Evolution of time-averaged recirculation area $\frac{A_{\text{rec}}}{A_0}$ as a function of the frequency for $Re_h = 2070$ $(\times)$ and $Re_h = 2900$ $(+)$ with $dc = 50\%$ and $a_0 = 0.040$.

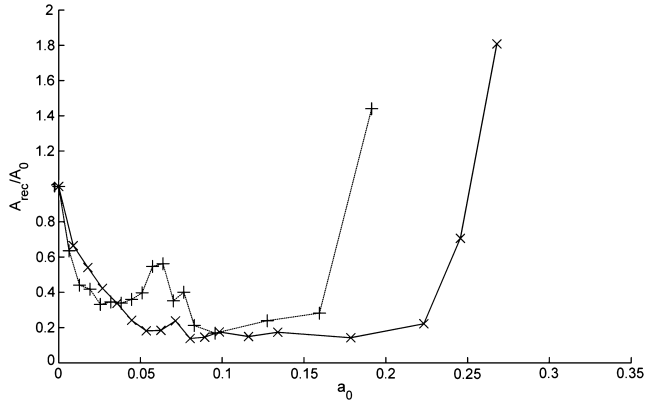

Fig. 6. Evolution of the time-averaged recirculation area $\frac{A_{\text{rec}}}{A_0}$ as a function of a_0 for $Re_h = 2070$ $(\times)$ and $Re_h = 2900$ $(+)$ with $F^+ \approx 1$ and $dc = 50\%$.

can clearly see that there is an optimal amplitude for the jet: if too small or too large, the control looses its efficiency, the optimum ratio being around $a_0 \approx 0.1$. In this case, the reduction of the recirculation area is even larger, close to 85%.

These results highlight the main difference between edge and upstream jet actuation. Similarly to edge injection, a minimal jet amplitude is required to affect the flow. However, for upstream actuation, the recirculation area increases with increasing jet amplitude instead of decreasing. Indeed, for high amplitudes, the jet fully penetrates the cross-flow, effectively becoming an obstacle to the incoming flow, leading to a massive increase in the recirculation area. One also notes that the flow's behavior is similar for both Reynolds numbers. Once again, while the recirculation area of the controlled mean field is near 0%, the mean recirculation area is closer to 10% of the uncontrolled values.

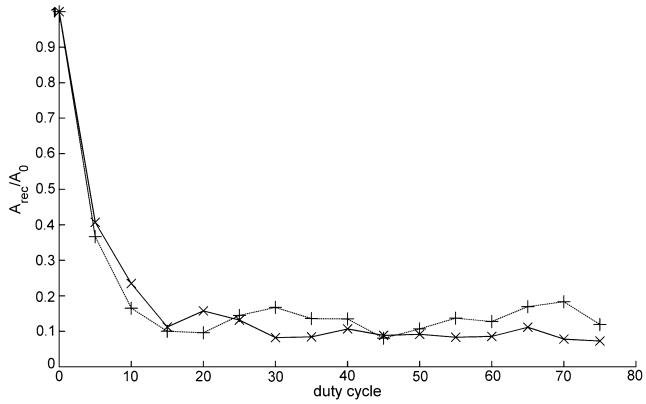

Fig. 7. Time-averaged recirculation area as a function of the duty cycle for $Re_h = 2070$ ($\times$) and $Re_h = 2900$ ($+$) with $F^+ \approx 1$ and $a_0 = 0.083$.

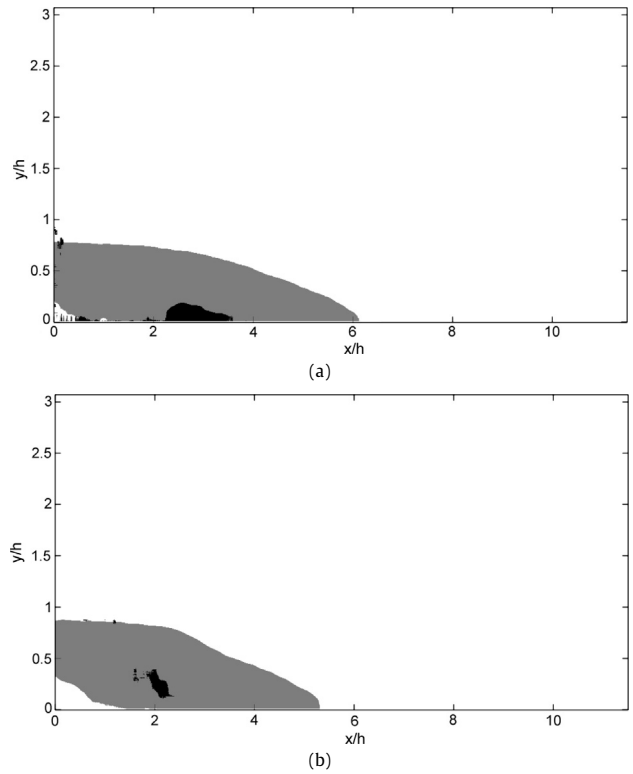

Fig. 8. (a) Comparison of time-averaged recirculation area obtained for $Re_h = 2070$ for uncontrolled (gray) and controlled (black) configurations ($F^+ \approx 1$, $dc = 20$, $a_0 = 0.083$). (b) Comparison of time-averaged recirculation area obtained for $Re_h = 2900$ for uncontrolled (gray) and controlled (black) configurations ($F^+ \approx 1$, $dc = 20$, $a_0 = 0.088$).

3.3. Influence of the duty cycle

Fig. 7 shows the evolution of the recirculation area as a function of the duty cycle for both Reynolds numbers and for the optimal actuation frequency and amplitude previously found.

Recirculation reduction area is increased, reaching nearly 90%. A minimal duty cycle of 10% is required to fully affect the flow, much lower than the usual 50% used in most of the previous studies. This is an important result: the duty cycle can be brought down significantly while still maintaining an effective control and then allowing a strong improvement of the overall energy balance between the power used by the actuation and the power gain (if related to a drag decrease, for instance).

3.4. Recirculation suppression

It appears that one major difference between the recirculation area and the recirculation length is its sensitivity to actuation. While the recirculation length can be reduced by 40%, the recirculation area can be reduced by nearly 90%. To explain this, velocity fields were computed with optimal parameters for both Reynolds numbers. Figs. 8a and 8b show the recirculation area of the mean field in the

uncontrolled and optimally controlled cases. On average, there is very little recirculation in the controlled cases. Indeed, the recirculation area can be almost null, while the recirculation length remains significant.

These figures illustrate how, in the mean sense, recirculation can be canceled through targeted control. Presumably the same results could be obtained using a pulsed actuation at the step edge, but it has to be confirmed.

4. Conclusion

The flow downstream of a backward-facing step controlled by an upstream pulsed jet was experimentally studied in a hydrodynamic channel. A measure of the recirculation area downstream of the BFS was introduced and used to quantify the effect of actuation for several flow configurations. The parametric space formed by jet amplitude, actuation frequency and duty cycle was explored for Reynolds numbers $Re_h = 2070$ and $Re_h = 2900$.

Results show recirculation can be greatly reduced, and in some cases nearly suppressed, for a fairly wide ranges of actuation parameters. Furthermore, while this phenomenon is clearly observed when considering the recirculation area, it can be missed when considering only the recirculation length. It emphasizes the importance of properly choosing the criterion used to evaluate the state of the separated flow. The recirculation area gives a more global evaluation of the state of the flow than the recirculation length.

The investigation of jet amplitude shows that, in the same way as injection at the step edge, a minimal jet amplitude is required to better control the flow. However, step injection and upstream injection differ at high jet amplitudes. In contrast to step injection where it has been shown that raising jet amplitude merely increases actuation effectiveness, albeit with diminishing returns, upstream injection jet amplitude reaches a threshold above which recirculation is greatly increased instead of decreased. In the case of upstream actuation, an optimal jet amplitude can be found.

Finally actuation is shown to be effective over a wide range of duty cycles, reaching a reduction of the recirculation area close to 90%. Moreover, it is shown that the duty cycle can be lowered to 10% while keeping recirculation at a minimum. Furthermore it is likely this limit is a consequence of the imperfect nature of the actuator. A better actuator could achieve lower duty cycles. Thus performances can be maintained while considerably lowering flow rate injection, and therefore energy expenditure. This result is of great interest for flow control applications where energy balance is a crucial point.

Acknowledgement

The DGA (Direction générale de l'armement, France) is gratefully acknowledged for financial support (grant no. 2011-170914/DGA/DS/MRIS).

References

[1] R.L. Simpson, Aspect of turbulent boundary layer separation, Prog. Aerosp. Sci. 32 (1996) 457–521.
[2] W.D. Hucho, Aerodynamic of Road Vehicles, Vieweg, Braunschweig, Germany, 2005.
[3] C.O. Paschereit, E. Gutmark, W. Weisenstein, Excitation of thermoacoustic instabilities by the interaction of acoustics and unstable swirling flow, AIAA J. 38 (2000) 1025–1034.
[4] B.F. Armaly, F. Durst, J.C.F. Pereira, B. Schonung, Experimental and theoretical investigation of backward-facing step flow, J. Fluid Mech. 127 (1983) 473–496.
[5] L. Hung, M. Parviz, K. John, Direct numerical simulation of turbulent flow over a backward-facing step, J. Fluid Mech. 330 (1997) 349–374.
[6] J.-F. Beaudoin, O. Cadot, J.-L. Aider, J.E. Wesfreid, Three-dimensional stationary flow over a backwards-facing step, Eur. J. Mech. 38 (2004) 147–155.
[7] J.-L. Aider, A. Danet, M. Lesieur, Large-eddy simulation applied to study the influence of upstream conditions on the time-dependant and averaged characteristics of a backward-facing step flow, J. Turbul. 8 (2007).
[8] A. Darabi, I. Wygnanski, Active management of naturally separated flow over a solid surface. Part 1. The forced reattachment process, J. Fluid Mech. 510 (2004) 105–129.
[9] H. Fiedler, H.H. Fernholz, On the management and control of turbulent shear flows, Prog. Aerosp. Sci. 72 (1990) 305–387.
[10] K.B. Chun, H.J. Sung, Control of turbulent separated flow over a backward-facing step by local forcing, Exp. Fluids 21 (1996) 417–426.
[11] V. Uruba, P. Jonas, O. Mazur, Control of a channel-flow behind a backward-facing step by suction/blowing, Heat Fluid Flow 28 (2007) 665–672.
[12] S. Narayan, B.R. Noack, A. Banaszuk, A.I. Khibnik, Active separation control concept: dynamic forcing of induced separation using harmonically related frequency, March 2002.
[13] R.T. M'Closkey, J.M. King, L. Cortelezzi, A.R. Karagozian, The actively controlled jet in crossflow, J. Fluid Mech. 452 (2002) 325–335.
[14] A. Eroglu, R.E. Breidenthal, Structure, penetration, and mixing of pulsed jets in crossflow, AIAA J. 39 (2001) 417–423.
[15] M. Pastoor, L. Henning, B.R. Noack, R. King, G. Tadmor, Feedback shear layer control for bluff body drag reduction, J. Fluid Mech. 608 (2008) 161–196.
[16] L. Henning, R. King, Robust multivariable closed-loop control of a turbulent backward-facing step flow, J. Aircr. 44 (1) (2007) 201–208.
[17] D. Sipp, A. Barbagallo, P. Schmid, Closed-loop control of an unstable open cavity, J. Fluid Mech. 641 (2010) 1–50.
[18] N. Gautier, J.-L. Aider, Control of the flow behind a backwards facing step with visual feedback, Proc. R. Soc. Lond. (2013), submitted for publication, available at arXiv.
[19] B.D. Lucas, Generalized image matching by the method of differences, PhD, Carnegie Mellon University, Pittsburgh, PA, USA, 1984.
[20] F. Champagnat, A. Plyer, G. Le Besnerais, B. Leclaire, S. Davoust, Y. Le Sant, Fast and accurate PIV computation using highly parallel iterative correlation maximization, Exp. Fluids 50 (2011) 1169–1182.
[21] S. Davoust, L. Jacquin, B. Leclaire, Dynamics of $m = 0$ and $m = 1$ modes and of streamwise vortices in a turbulent axisymmetric mixing layer, J. Fluid Mech. 709 (2012) 408–444.
[22] F. Sartor, G. Losfeld, R. Bur, PIV study on a shock-induced transition in subsonic flow, Exp. Fluids 53 (2012) 815–827.
[23] M.S. Chong, A.E. Perry, B.J. Cantwell, A general classification of 3-dimensional flow fields, Phys. Fluids 2 (1990) 765–777.
[24] J. Zhou, R.J. Adrian, S. Balachandar, T.M. Kendall, Mechanisms for generating coherent packets of hairpin vortices, J. Fluid Mech. 387 (1999) 353–396.